QUASI-PERIODIC OSCILLATION OF A CORONAL BRIGHT POINT

TANMOY SAMANTA[1], DIPANKAR BANERJEE[1], AND HUI TIAN[2]
[1] Indian Institute of Astrophysics, Koramangala, Bangalore 560034, India; tsamanta@iiap.res.in
[2] Harvard-Smithsonian Center for Astrophysics, 60 Garden Street, Cambridge, MA 02138, USA; hui.tian@cfa.harvard.edu

ABSTRACT

Coronal bright points (BPs) are small-scale luminous features seen in the solar corona. Quasi-periodic brightenings are frequently observed in the BPs and are generally linked with underlying magnetic flux changes. We study the dynamics of a BP seen in the coronal hole using the Atmospheric Imaging Assembly images, the Helioseismic and Magnetic Imager magnetogram on board the *Solar Dynamics Observatory*, and spectroscopic data from the newly launched Interface Region Imaging Spectrograph (IRIS). The detailed analysis shows that the BP evolves throughout our observing period along with changes in underlying photospheric magnetic flux and shows periodic brightenings in different EUV and far-UV images. With the highest possible spectral and spatial resolution of IRIS, we attempted to identify the sources of these oscillations. IRIS sit-and-stare observation provided a unique opportunity to study the time evolution of one footpoint of the BP as the slit position crossed it. We noticed enhanced line profile asymmetry, enhanced line width, intensity enhancements, and large deviation from the average Doppler shift in the line profiles at specific instances, which indicate the presence of sudden flows along the line-of-sight direction. We propose that transition region explosive events originating from small-scale reconnections and the reconnection outflows are affecting the line profiles. The correlation between all these parameters is consistent with the repetitive reconnection scenario and could explain the quasi-periodic nature of the brightening.

Key words: Sun: corona – Sun: magnetic fields – Sun: oscillations – Sun: transition region – Sun: UV radiation

Supporting material: animations

1. INTRODUCTION

Coronal bright points (BPs) are bright dynamical features seen in quiet-Sun and coronal holes (CHs). The dynamics and evolution were studied in X-rays and EUV wavelengths (Vaiana et al. 1973; Golub et al. 1974, 1976a, 1976b; Habbal & Withbroe 1981; Zhang et al. 2001, 2012; Tian et al. 2008a; Li et al. 2013). They generally live for a few hours to a few days and have sizes less than $50''$. BPs are believed to be composed of loops connected locally with the photospheric bipolar magnetic fields (Golub et al. 1976b; Sheeley & Golub 1979). With recent high-resolution EUV images it is clear that a BP is not a point or simple loop-like structure but looks like a miniature active region with multiple magnetic poles with several connectivities. Moreover, depending on the emergence and cancellation of the magnetic polarities, the BPs evolve with time and show a lot of dynamics. The theoretical model argues that the interaction between two opposite polarities creates an X-point magnetic reconnection that locally heats the corona and produces BPs (Parnell et al. 1994; Priest et al. 1994). The locations of BPs appear to be related to the giant convection cells (McIntosh et al. 2014). Zhang et al. (2012, 2014) suggested that small bipolar emerging magnetic loops might reconnect with an overlying large loop or open field lines and produce brightenings. They also proposed that BPs might consist of two components: one is a long-lived smooth component due to gentle quasi-separatrix layer reconnections, and the other is a quasi-periodic impulsive component, called BP flashes.

Sheeley & Golub (1979) reported that the BPs evolve with a 6-minute timescale. Several observations in X-ray and EUV show periodic variation in the intensity of BPs over a broad range of periodicity (Nolte et al. 1979; Sheeley & Golub 1979;

Habbal & Withbroe 1981; Strong et al. 1992; Kumar et al. 2011; Tian et al. 2008b; Kariyappa et al. 2011; Chandrashekhar et al. 2013). Some suggested that these oscillations are caused by the leakage of acoustic waves (*p*-modes), which propagate along the magnetic flux tubes and convert into magnetoacoustic mode at higher atmosphere (Bogdan et al. 2003; Kuridze et al. 2008; Srivastava & Dwivedi 2010). Others believe that the intensity oscillations are due to repeated magnetic reconnections (Madjarska et al. 2003; Ugarte-Urra et al. 2004; Doyle et al. 2006).

Several studies have been carried out to understand the periodic nature, but their origin remains inconclusive. Here we study a BP inside a CH as seen in the Atmospheric Imaging Assembly (AIA) EUV coronal images (Lemen et al. 2012) and in the Helioseismic and Magnetic Imager (HMI) magnetogram (Schou et al. 2012) on the *Solar Dynamics Observatory* and simultaneously with the newly launched Interface Region Imaging Spectrograph (IRIS) (De Pontieu et al. 2014). Combining imaging and spectroscopic observations, we study the dynamical changes within this BP and its variability. We show that the time variability can be explained in terms of a repeated magnetic reconnection scenario.

2. DATA ANALYSIS AND RESULTS

2.1. Observation and Data Reduction

Observational data were obtained from IRIS, AIA, and HMI instruments from 5:14 to 6:34 UT on 2014 May 11. We used AIA images centered at 335, 193, 171, and 1600 Å. AIA and HMI images have $0\farcs6$ pixel size and were co-aligned. IRIS data were taken in sit-and-stare mode. It was pointing toward a CH (centered at $404''$, $-612''$). Slit-jaw images (SJIs) were available only with the 1330 Å filter. We have used IRIS Level
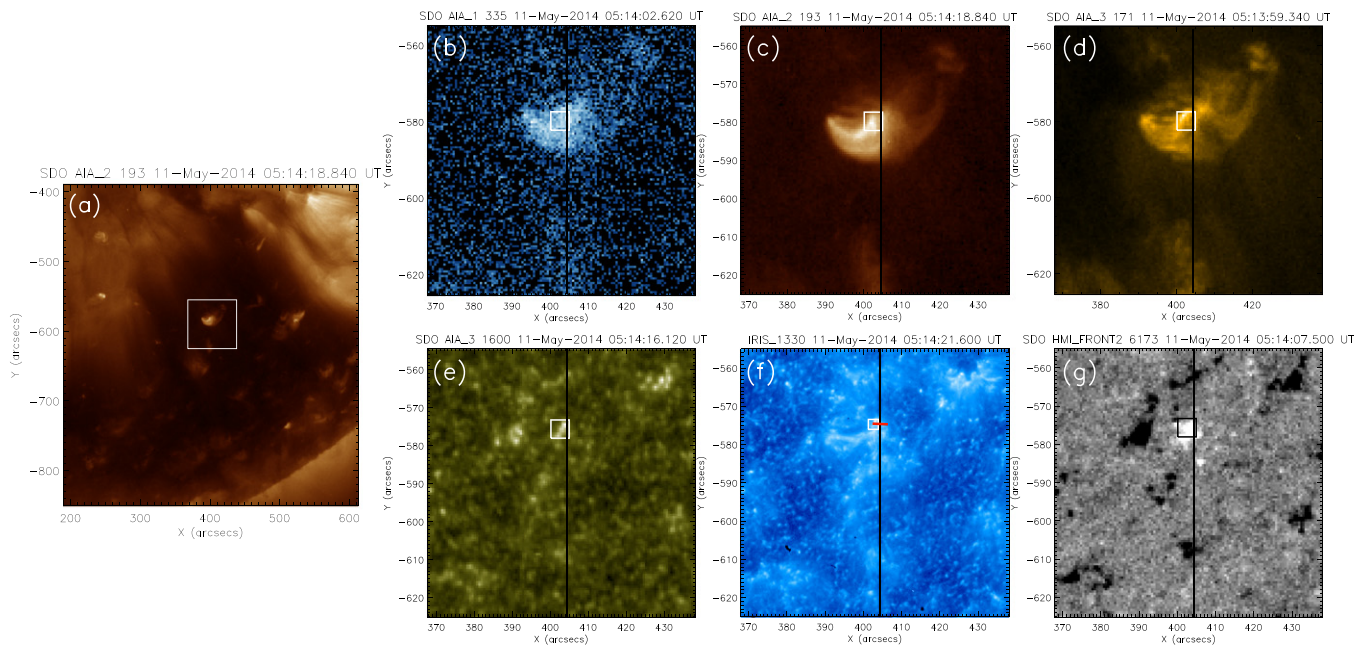
Figure 1. (a): AIA 193 Å image showing a coronal hole. The white box represents our region of interest (ROI), covering a bright point in the coronal hole. Zoomed views of the ROI as recorded by different AIA channels are shown in (b)–(e), (f) shows the IRIS 1330 Å SJI, and (g) shows the HMI line-of-sight (LOS) magnetogram. The vertical black line on each image represents the position of the IRIS slit. Intensities within the small white box of (b)–(f) are used to study oscillation properties (see Figure 3). The red horizontal tick marked on the IRIS 1330 Å image (f) is the location where we study the variation of different line parameters of the Si IV $\lambda1393.76$ line (see Figure 4).
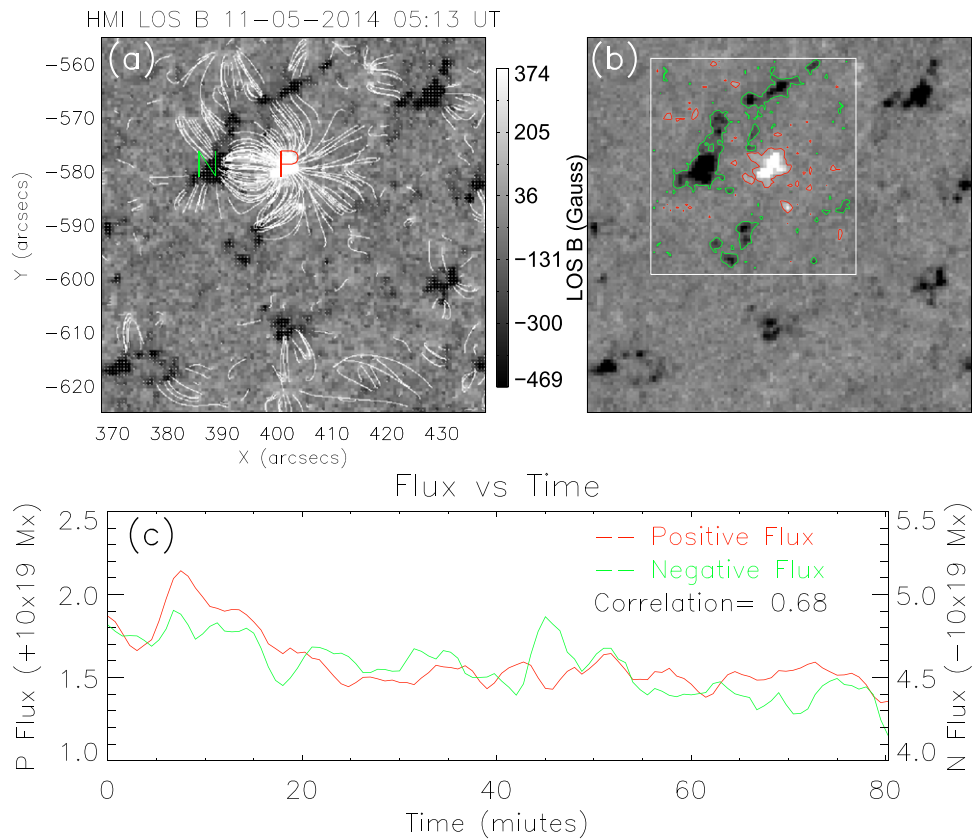
(An animation of this figure is available.)

Figure 2. (a) HMI LOS magnetogram and extrapolated potential field lines (white lines). (b) On the same magnetogram the red and green contours represent the field above +20 and −20 G, respectively. The magnetic fluxes (positive and negative) are calculated within the contours (red and green, respectively) inside the rectangular white box. (c) Variation of measured positive and negative flux over time.
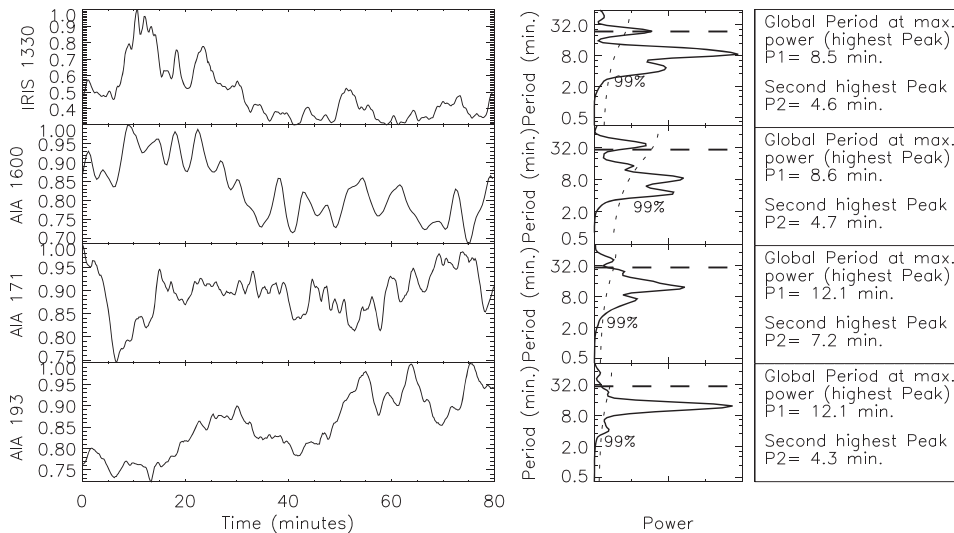
Figure 3. In each row the left panel shows the variation of intensities of different AIA and IRIS channels. The middle panel shows the global wavelet power spectrum. The confidence levels are overplotted with dashed lines. The right panels show the significant periods as measured from the global wavelet spectrum. Intensity variations of AIA images and IRIS 1330 Å SJIs are calculated from the region inside the white boxes as shown in the Figures 1(b)–(f).

2 processed data, which takes care of dark current, flat field, geometrical corrections, etc. The exposure time and cadence of 1330 Å SJIs and spectra were 8 and 9.6 s, respectively. IRIS has a pixel size of $0''166$. AIA and HMI data were then co-aligned with IRIS data. IRIS 1330 Å and AIA 1600 Å were used for co-alignment. De-rotation was performed on all AIA and HMI images to co-align the data cubes.

Figure 1(a) shows the CH in the AIA 193 Å image. The magnetogram (Figure 1(g)) shows that the CH is dominated by negative-polarity magnetic field (color bar can be seen in Figure 2). We made a 48 hr movie with AIA 193 Å images and HMI magnetograms with 1 hr cadence. It reveals that the BP appears around 16:00 UT on 2014 May 10 with emergence of some positive flux and disappears around 17:00 UT on 2014 May 12 (with a lifetime ~38 hr) with the complete disappearance of the positive flux. The positive flux concentration within this BP over the dominated background negative flux is the probable reason of the existence of the BP. Figure 1 shows the BP as seen in various AIA channels (b–e), IRIS 1330 Å SJI (f), and HMI line-of-sight (LOS) magnetogram (g). The vertical black line on each image represents the position of the IRIS slit. It clearly shows that the IRIS slit is crossing one footpoint of the BP, where the magnetic field is positive.

2.2. Magnetic Field Evolution

Figure 2(a) shows the HMI LOS magnetogram. Potential field extrapolation was performed by assuming a constant α force-free magnetic field (with $\alpha = 0$) (Nakagawa & Raadu 1972; Alissandrakis 1981). The white lines connecting different polarities ($\geqslant \pm 20$ G) represent the extrapolated field lines. Strong connectivity between primary polarity P (positive) and N (negative) can be seen. It agrees well with the intensity images as seen in IRIS SJIs and AIA images. Our ROI lies well within a CH, primarily dominated by negative flux over the entire region. Based on the main connectivity with the positive flux (P), we have selected a region marked as a white box in Figure 2(b) to calculate the magnetic flux. Contours with +20 and −20 G are drawn in red and green, respectively, and fluxes are calculated within these contours.

After calculating the fluxes for each time frame, smoothed over three frames, light curves (LCs) are shown in Figure 2(c). There appears to be a good correlation between positive and negative flux, with a correlation coefficient (CC) of 0.68. It indicates that both positive and negative flux amplitudes vary in a similar manner. Movie 1 (available online) shows small-scale magnetic flux emergence and cancellation. It is possible that newly emerging small bipolar loops are reconnecting with the overlying preexisting large loop (P–N) as suggested by Priest et al. (1994) and Zhang et al. (2012, 2014), which could explain the good correlation. In Section 2.4, we show signatures of reconnection and their relation with flux changes.

2.3. Imaging Observations

We have focused on the dynamics of one footpoint (positive polarity P). We study the time evolution of this small region as seen with simultaneous multiwavelength images corresponding to the transition region (TR) and coronal layers. We have computed average intensities inside the small white box on top of the footpoint as shown in Figures 1(b)–(f). The size of the white box in AIA was 8×8 pixels $(\sim(4''8)^2)$, and IRIS was 15×15 pixels $(\sim(2''5)^2)$. AIA box size was selected slightly larger to accommodate the loop expansion higher up and also to reduce movement effects of the loop if any. The smoothed LCs over three time frames are shown in Figure 3. Left panels show (from top to bottom) the LCs of IRIS 1330 Å and AIA 1600 Å, 171 Å, and 193 Å, respectively. We have performed wavelet analysis (Torrence & Compo 1998) on each LC after removing the background trend. We use the Morlet function, a complex sine wave modulated by a Gaussian, for convolution with the time series in the wavelet transform. The global wavelet power spectra are shown in the middle panel of Figure 3. A confidence level of 99% is overplotted by the dotted white line. The confidence level was set by assuming white noise (Torrence & Compo 1998). Measured periods are printed in the right panels. The global wavelet power plots clearly show the presence of periodicities. A dominant period around 8 minutes is present in IRIS 1330 Å and AIA 1600 Å and 171 Å LCs. Though the global wavelet plots of AIA 171 Å
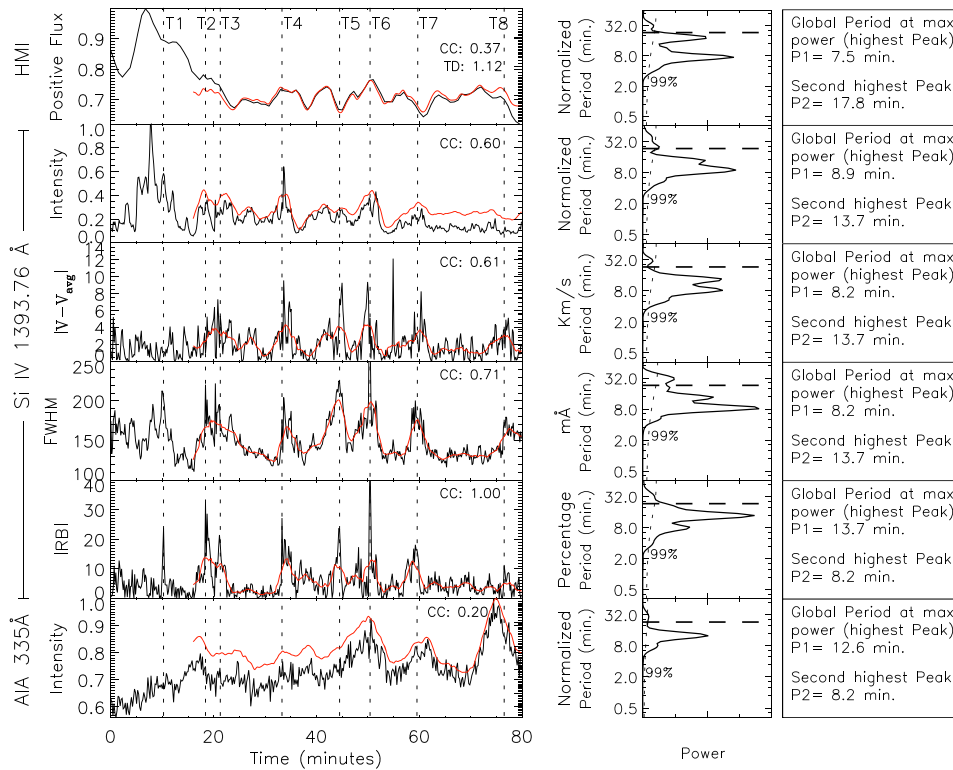
Figure 4. Similar to Figure 3, the top row corresponds to HMI positive flux, the bottom row corresponds to AIA 335 Å intensity, and other rows correspond to different line parameters as calculated from the Si IV λ1393.76 line profiles. |RB| and $|V - V_{avg}|$ represent absolute RB asymmetry and the deviation from average Doppler shift, respectively, where V_{avg} is the average Doppler shift. Red lines are the trend-subtracted smoothed curves for duration 16–80 minutes. Si IV λ1393.76 line profiles correspond to the location as marked in Figure 1(f), with the red tick mark on the IRIS 1330 Å SJI. The CC between all the LCs with the absolute RB is printed in the respective panel.

and 193 Å show the presence of strongest peak at ∼12 minutes, there is a weaker power around 8 minutes.

Now we try to explore the source of these oscillations. Several observational evidences show a positive correlation between the EUV and X-ray emission with the underlying photospheric magnetic flux (Preś & Phillips 1999; Handy & Schrijver 2001; Ugarte-Urra et al. 2004; Pérez-Suárez et al. 2008). Preś & Phillips (1999) have observed that X-ray and EUV emissions are temporally correlated with the photospheric magnetic flux. They also suggested the possibility of several small "network flares" occurring during the lifetime of these BPs. Chandrashekhar et al. (2013) have found a good temporal correlation between magnetic flux associated with the footpoints and the intensity brightening and suggested the possibility of a repeated reconnection scenario. Note that most of these were imaging observations. In the following subsection we study the time evolution from the IRIS spectroscopic data, which provides additional information on the possible sources of these oscillations. IRIS sit-and-stare observation provides an ideal opportunity to study the time evolution of this footpoint as the slit position is crossing it.

2.4. Spectroscopic Analysis

At first, a single Gaussian fit was performed on the averaged (over all the pixels along the slit and time) profile of the photospheric Si I λ1401.513 line for absolute calibration of wavelength. Now, for our spectroscopic study, we have selected a position $(402\farcs40, -574\farcs52)$ that corresponds to one footpoint of the BP loop system. The position is marked by

a red tick mark on the IRIS 1330 Å SJI in Figure 1(f). An average over 3 pixels along the slit and a running average of three points along dispersion were applied to the spectra to improve signal-to-noise ratio. After that, a single Gaussian fit was applied to each IRIS Si IV λ1393.76 line profile to derive line intensity, Doppler shift, and FWHM of the line. To compute the asymmetry in the line profile, we performed red–blue (RB) asymmetry analysis (De Pontieu et al. 2009; Martínez-Sykora et al. 2011; Tian et al. 2011b). A single Gaussian fit was performed only in the core of the profile to find the line centroid (similar to that in Tian et al. 2014). Red and blue wings were then subtracted and normalized to peak intensity to construct the RB asymmetry profile (in percentage). Finally, we have constructed the RB asymmetry LC by taking the average over the 15–40 km s^{-1} velocity range for each profile. Positive and negative values represent enhancements in the red and blue wings, respectively.

Now, the variation of all the line parameters with time, along with HMI positive flux and AIA 335 Å intensity, is shown in Figure 4. Different rows (from top to bottom) correspond to HMI positive flux, intensity, deviation from average Doppler shift $(|V - V_{avg}|)$, FWHM, absolute RB asymmetry (|RB|) of the Si IV λ1393.76 line, and AIA 335 Å intensity, respectively. Now for the correlation studies between different parameters and to find out the periodic nature, we have selected a time interval of 16–80 minutes. The initial rapid change in flux affects the power analysis, so we have omitted the first 16 minutes for this analysis. We use trend-subtracted smoothed LCs, as represented by red lines in Figure 4, for easier comparison. The wavelet analysis was applied over the
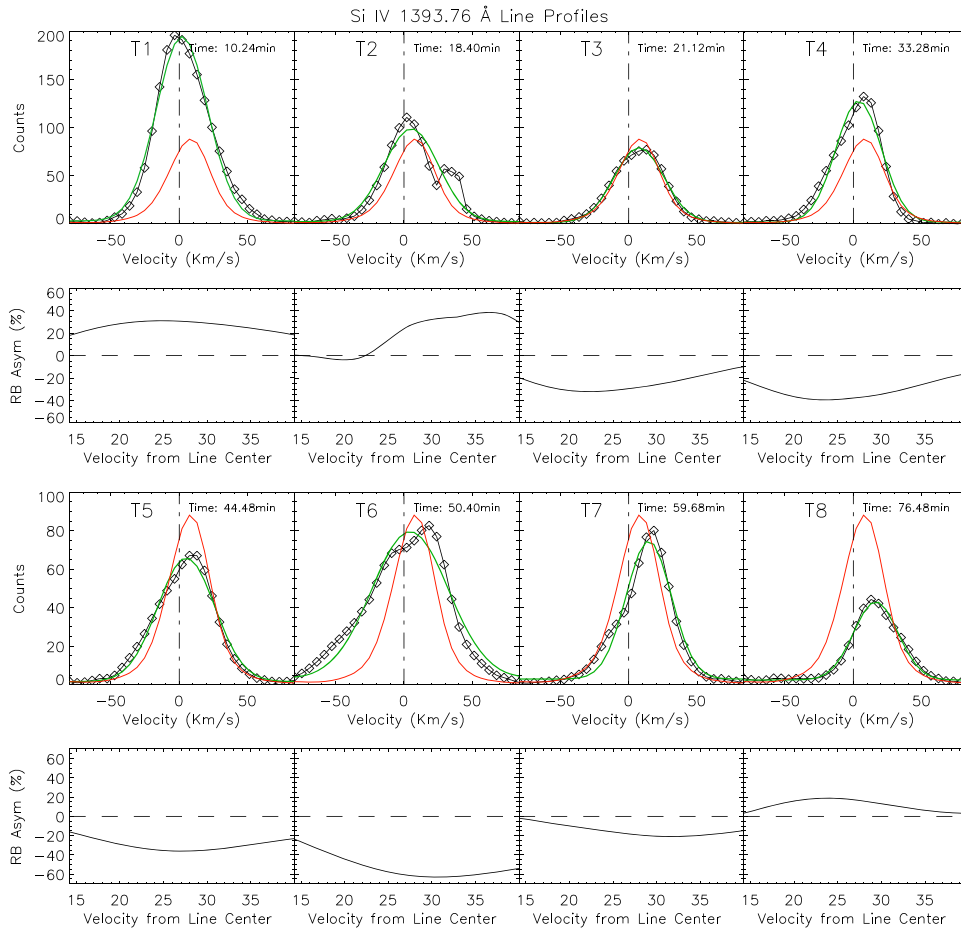
Figure 5. Line profiles of the Si IV λ1393.76 line at various instances as labeled along with their corresponding RB asymmetry profile (from 15 to 40 Km s^{-1}) in the bottom. Red lines represent average line profiles over time. Green lines are the Gaussian fits.

(An animation of this figure is available.)

smoothed curve to investigate the oscillation properties. Global wavelet power spectra, along with 99% confidence level, are shown in the middle panels. Observed periodicities are then printed on the right side. The power analysis on the line parameters shows the omnipresence of a strong periodicity around 8 and 13 minutes. CCs of all the line parameters with the absolute RB asymmetry are printed in each panel. We correlate different LCs with the RB asymmetry LC as the RB asymmetry provides a good measurement of the distortion in line profile form Gaussian. To investigate it further, we will focus on specific instances and will have a closer look at the variation of line profiles. We notice sudden changes in the line parameters at certain times. In Figure 4, horizontal grids represent the particular instances where certain changes occur. The line profiles at T1, T2, T3, T4, T5, T6, T7, and T8 time instances are shown in Figure 5, along with averaged (in red) and Gaussian fit (in green) profiles. The RB asymmetry profiles are shown in the lower panel. It clearly shows strong asymmetry in the profiles at those particular instances due to the existence of some secondary emission component. Movie 2 (available online) shows the evolution of the line profiles.

The correlation between intensity, FWHM, $|V - V_{avg}|$, and $|RB|$ can be easily explained in terms of sudden flows along the line of sight. In active region boundaries, all the line parameters coherently change due to quasi-periodic upflows in the medium (De Pontieu & McIntosh 2010; Tian

et al. 2011a, 2012). In our study, we observed both red- and blueward asymmetries from time to time (see Figure 5), which is different from active region boundary studies, where predominantly blueward asymmetry is reported. Our observations can be explained in terms of both high-speed upflows and downflows. Transition region explosive events (EEs) could be a possible explanation (Brueckner & Bartoe 1983; Dere et al. 1989; Innes et al. 1997; Chae et al. 1998; Teriaca et al. 2004; Huang et al. 2014). EEs are believed to result from reconnection, which will affect the line profiles. Reconnection jets (regardless of the direction) usually lead to enhancements at the line wing (or wings), which would lead to large RB values, larger line width, and larger intensity. The presence of these additional flow components usually also leads to large perturbation of the Doppler shift. This sudden change in the line parameters is consistent with the behavior of bursty EEs. We find the periodic occurrence of EEs at one footpoint of a coronal BP. The observed periodicities at one footpoint of the BP at the different temperature channels are similar to the observed periodic changes in different line parameters, which may indicate that recurring EEs are likely producing the oscillatory signal seen in the BP.

Chae et al. (1998) reported that EEs happen preferentially in regions with weak and mixed-polarity magnetic fluxes. They also noticed that the majority of EEs occur during the cancellation of photospheric magnetic field. In our study, we

find a correlation between RB asymmetry and underlying positive flux. We use a cross-correlation technique to find out whether the two LCs are showing a similar variation with some time delay (similar to Tian et al. 2012). It shows that the |RB| LC has a time delay (TD) of 1.12 minutes from the magnetic flux LC. Hence, It can be conjectured that the line profiles are strongly affected during the magnetic flux cancellation phase. It could be that the new emerging flux reconnects with the preexisting field, which cancels the local flux and creates EEs. The periodic behavior might be explained by repeated reconnection. One can also notice, while carefully looking at the variations, that the RB asymmetry does not change randomly; it changes slowly with a sharp increase around specific instances and then slowly decreases. This matches well with a slow reconnection scenario (Wang & Shi 1993). Slow magnetic reconnections occurring in the lower atmosphere could initiate fast reconnection in the TR and then decrease slowly. After some relaxation time, it repeats.

We also searched for the signature of heating due to reconnections. The AIA 335 Å channel corresponds to an ionization temperature of about 2.5×10^6 K, with a wide temperature response. In Figure 4, the 335 Å LC shows an increase of intensity during the time when the line profiles show sudden changes. Due to reconnection, magnetic energy releases and heats the medium locally at the TR. This localized heating close to the reconnection point may increase the temperature at certain pockets in the TR, and AIA may see some of these emissions. Hence, depending on the heating, higher-temperature emission can enhance during the reconnection time. The AIA 335 Å LCs show similar properties. We wish to address this conjecture in our future work while looking at coronal spectral lines.

3. CONCLUSION

We study the dynamics of a BP within a CH using combined imaging, spectroscopic, and magnetic measurements. We focused our analysis on one footpoint of a bipolar loop structure. Throughout our observation, both positive and negative magnetic flux shows correlated variations. This may suggest that emerging flux interacts with the preexisting overlying fields, which results in reconnection and cancellation of the flux at the site of the BP. We conjecture that the periodic behavior of the positive flux may correspond to repeated reconnections, which leads to a series of continuous periodic brightenings as seen in different EUV and far-UV lines. We propose that EEs are created due to X-point magnetic reconnection and resultant outflows generally affect the line profiles. The presence of the secondary component emission in the line profiles confirms that. Furthermore, we observed enhanced line profile asymmetry, enhanced line width, and a large deviation from the average Doppler shift at specific instances. The correlation between all these parameters is consistent with the scenario of repetitive alteration of the line profile by bursty reconnection outflows. We observe similar periodicities not only at different line parameters of the Si IV line but also with AIA channels, and they are concurrent in time and space and hence seem to be related. During EEs (see Figure 4), we see a corresponding change in the magnetic field —this is a one-to-one correspondence and certainly indicates the close relationship between the two.

REFERENCES

Alissandrakis, C. E. 1981, A&A, 100, 197
Bogdan, T. J., Carlsson, M., Hansteen, V. H., et al. 2003, ApJ, 599, 626
Brueckner, G. E., & Bartoe, J.-D. F. 1983, ApJ, 272, 329
Chae, J., Wang, H., Lee, C.-Y., Goode, P. R., & Schühle, U. 1998, ApJL, 497, L109
Chandrashekhar, K., Krishna Prasad, S., Banerjee, D., Ravindra, B., & Seaton, D. B. 2013, SoPh, 286, 125
De Pontieu, B., & McIntosh, S. W. 2010, ApJ, 722, 1013
De Pontieu, B., McIntosh, S. W., Hansteen, V. H., & Schrijver, C. J. 2009, ApJL, 701, L1
De Pontieu, B., Title, A. M., Lemen, J. R., et al. 2014, SoPh, 289, 2733
Dere, K. P., Bartoe, J.-D. F., Brueckner, G. E., & Recely, F. 1989, ApJL, 345, L95
Doyle, J. G., Popescu, M. D., & Taroyan, Y. 2006, A&A, 446, 327
Golub, L., Krieger, A. S., Silk, J. K., Timothy, A. F., & Vaiana, G. S. 1974, ApJL, 189, L93
Golub, L., Krieger, A. S., & Vaiana, G. S. 1976a, SoPh, 49, 79
Golub, L., Krieger, A. S., & Vaiana, G. S. 1976b, SoPh, 50, 311
Habbal, S. R., & Withbroe, G. L. 1981, SoPh, 69, 77
Handy, B. N., & Schrijver, C. J. 2001, ApJ, 547, 1100
Huang, Z., Madjarska, M. S., Xia, L., et al. 2014, ApJ, 797, 88
Innes, D. E., Inhester, B., Axford, W. I., & Wilhelm, K. 1997, Natur, 386, 811
Kariyappa, R., Deluca, E. E., Saar, S. H., et al. 2011, A&A, 526, A78
Kumar, M., Srivastava, A. K., & Dwivedi, B. N. 2011, MNRAS, 415, 1419
Kuridze, D., Zaqarashvili, T. V., Shergelashvili, B. M., & Poedts, S. 2008, AnGeo, 26, 2983
Lemen, J. R., Title, A. M., Akin, D. J., et al. 2012, SoPh, 275, 17
Li, D., Ning, Z. J., & Wang, J. F. 2013, NewA, 23, 19
Madjarska, M. S., Doyle, J. G., Teriaca, L., & Banerjee, D. 2003, A&A, 398, 775
Martínez-Sykora, J., De Pontieu, B., Hansteen, V., & McIntosh, S. W. 2011, ApJ, 732, 84
McIntosh, S. W., Wang, X., Leamon, R. J., & Scherrer, P. H. 2014, ApJL, 784, L32
Nakagawa, Y., & Raadu, M. A. 1972, SoPh, 25, 127
Nolte, J. T., Solodyna, C. V., & Gerassimenko, M. 1979, SoPh, 63, 113
Parnell, C. E., Priest, E. R., & Golub, L. 1994, SoPh, 151, 57
Pérez-Suárez, D., Maclean, R. C., Doyle, J. G., & Madjarska, M. S. 2008, A&A, 492, 575
Preś, P., & Phillips, K. H. J. 1999, ApJL, 510, L73
Priest, E. R., Parnell, C. E., & Martin, S. F. 1994, ApJ, 427, 459
Schou, J., Scherrer, P. H., Bush, R. I., et al. 2012, SoPh, 275, 229
Sheeley, N. R., Jr., & Golub, L. 1979, SoPh, 63, 119
Srivastava, A. K., & Dwivedi, B. N. 2010, MNRAS, 405, 2317
Strong, K. T., Harvey, K., Hirayama, T., et al. 1992, PASJ, 44, L161
Teriaca, L., Banerjee, D., Falchi, A., Doyle, J. G., & Madjarska, M. S. 2004, A&A, 427, 1065
Tian, H., Curdt, W., Marsch, E., & He, J. 2008a, ApJL, 681, L121
Tian, H., McIntosh, S. W., & De Pontieu, B. 2011a, ApJL, 727, L37
Tian, H., McIntosh, S. W., De Pontieu, B., et al. 2011b, ApJ, 738, 18
Tian, H., McIntosh, S. W., Wang, T., et al. 2012, ApJ, 759, 144
Tian, H., Xia, L.-D., & Li, S. 2008b, A&A, 489, 741
Tian, H., DeLuca, E. E., Cranmer, S. R., et al. 2014, Sci, 346, 1255711
Torrence, C., & Compo, G. P. 1998, BAMS, 79, 61
Ugarte-Urra, I., Doyle, J. G., Madjarska, M. S., & O'Shea, E. 2004, A&A, 418, 313
Vaiana, G. S., Davis, J. M., Giacconi, R., et al. 1973, ApJL, 185, L47
Wang, J., & Shi, Z. 1993, SoPh, 143, 119
Zhang, J., Kundu, M. R., & White, S. M. 2001, SoPh, 198, 347
Zhang, Q. M., Chen, P. F., Ding, M. D., & Ji, H. S. 2014, A&A, 568, A30
Zhang, Q. M., Chen, P. F., Guo, Y., Fang, C., & Ding, M. D. 2012, ApJ, 746, 19